

Selective compositional mixing in GaAs/AlGaAs superlattice induced by low dose Si focused ion beam implantation

P. Chen and A. J. Steckl^{a)}

Nanoelectronics Laboratory, Department of Electrical and Computer Engineering, University of Cincinnati, Cincinnati, Ohio 45221-0030

(Received 26 August 1994; accepted for publication 6 February 1995)

The Al-Ga interdiffusion induced by Si focused ion beam implantation and subsequent rapid thermal annealing (RTA) was investigated in an Al_{0.3}Ga_{0.7}As/GaAs superlattice structure with equal 3.5 nm barrier and well widths. Si⁺⁺ was accelerated to either 50 or 100 keV and implanted parallel to sample normal at doses ranging from 10¹³ to 10¹⁵/cm². The effect of rapid thermal anneal of 10 s at 950 °C was characterized by the secondary ion mass spectrometry technique. In the implanted region, the interdiffusion causing compositional mixing was significantly enhanced by the Si implantation. An ion dose as low as 1×10¹⁴/cm² results in a two-order of magnitude increase in the interdiffusion coefficient, to a value of 4.5×10⁻¹⁴ cm²/s, producing a mixing effectiveness of ~90%. In contrast, the RTA-only case produces an interdiffusion coefficient of 1.3×10⁻¹⁶ cm²/s and very little mixing. A strong depth dependence of the mixing process was observed at 100 keV implantation energy, with a "pinch-off" (more heavily mixed) region being formed at a certain depth. It is noticed that the depth where this enhancement occurred is not associated with either the maximum concentration of Si ions or of vacancies. Instead, it coincides with the positive maximum of the second derivative of the vacancy profile, which in turn represents a maximum in the vacancy injection generated by the presence of a transient vacancy concentration gradient. Based on these findings, a theoretical model was developed using vacancy injection as responsible for mixing. © 1995 American Institute of Physics.

I. INTRODUCTION

It is known that the compositional intermixing of AlGaAs/GaAs superlattice structures can be significantly enhanced by introducing certain species such as Si, Zn, Al, and Ga.¹ The energy band gap and the index of refraction, as well as other material properties, are altered in the mixed region to correspond to an alloy of the appropriate composition. Using this effect, optical devices such as distributed Bragg reflector (DBR) and distributed feedback (DFB) lasers, channel waveguides, quantum wires, and quantum dots can be fabricated by locally mixing the superlattice. Among the various approaches to implementing localized mixing, Si ion implantation in conjunction with subsequent thermal annealing has been proven to be one of the most efficient methods for inducing mixing. Focused ion beam (FIB) implantation technology has been especially attractive in this application, since it provides a maskless process with high spatial resolution.²

Many applications of superlattice mixing demand highly sophisticated control in both horizontal and vertical directions. Usually, minimal lateral spreading of the mixed region is required for implementation of fine features. For instance, a first order laser grating in the AlGaAs/GaAs material system requires a grating period of about 120 nm. Thus, the mixed region should not exceed 60 nm in width. Another example is quantum wires whose width is expected to be smaller than 20 nm. Therefore, the minimization of the lateral dimension of the mixed region is a serious consider-

ation. In general, the lateral resolution is limited by the precision of the pattern generation and/or transfer technology, the lateral profiles of the ion beam (and of the ions implanted in the solid), and by diffusion during the post-implantation annealing. The precision of pattern generation and/or transfer technology relies on the capability of the equipment. With FIB technology, fairly high spatial resolution can be achieved. However, the ultimate resolution is greatly dependent on ion beam profile and processing conditions such as ion energy, dose, and thermal annealing. To obtain a high resolution pattern, a low dose is preferred because it results in a laterally narrower mixed region and it reduces the implantation-induced damage. Rapid thermal annealing is frequently employed in order to minimize lateral diffusion, to preserve the sharpness of the heterointerface, and to simplify the process. Finally, a short period superlattice, which is more readily mixed, is advantageous for the same reasons.

In addition to optimization in the lateral direction, depth control of the mixed region in the vertical direction is also critical for a number of applications, for instance the gain-coupled grating in a DFB laser. Hence, a thorough understanding of the mixing mechanism is essential for precise control of the mixing process.

The occurrence of AlGaAs/GaAs intermixing results from Ga-Al interdiffusion during the thermal process. The interdiffusion of column III atoms is known to proceed through point defects of the crystal. Therefore, the presence of extra vacancies will enhance the interdiffusion and, in turn, the intermixing. Furthermore, as charged point defects are introduced via doping, the interdiffusion will be further enhanced due to the interaction between impurities and charged point defects. Under conditions of thermal equilib-

^{a)}Author to whom correspondence should be addressed; Electronic mail: a.steckl@uc.edu

rium, the charged point defect concentration is dependent on the crystal Fermi level.^{1,3} In this case, only the presence of the dopant, instead of its motion, is of importance.

Si implantation has proven to be one of the most efficient techniques for enhancing mixing. An appreciable research effort has addressed both the technique and the mechanisms of Si implantation enhanced mixing.^{4–20} Most of the early investigations were performed in conjunction with furnace annealing (FA) at temperatures of about 850 °C for a period of hours. Under this annealing process, the Si impurities diffuse significantly. This impurity diffusion was suggested^{7–9,12–14,20,21} to be responsible for the enhancement of Al-Ga interdiffusion under As overpressure. Despite the fact that the Fermi-level theory^{1,3} is a steady state model, it can still be applied to the Si impurity diffusion process³ during furnace annealing because the diffusion is relatively slow and therefore a dynamic equilibrium can be attained. With either the Fermi-level model or impurity diffusion model, the degree of interdiffusion is decided by the Si concentration which can be translated into a concentration of point defects. The diffusion due to furnace annealing is quite significant, usually resulting in a large lateral profile.

In conjunction with ion implantation, rapid thermal annealing is capable of producing efficient intermixing and provides a quick, simple, and localized process. In the rapid thermal anneal (RTA) time scale, impurities do not move appreciably.^{17–19} Hence, the impurity diffusion theory cannot be applied. Meanwhile, the condition of steady-state required for the Fermi-level effect model is usually not suitable in the RTA time frame, wherein thermal equilibrium may not be attained. Furthermore, the intermixing obtained after RTA does not occur in the region where Si concentration reaches its maximum, indicating that the impurity concentration is no longer the decisive factor in RTA. Evidently, the conclusions drawn from furnace annealing cannot explain the interdiffusion mechanism during the RTA process. Therefore, an interdiffusion model valid within the RTA time frame was proposed by Lee *et al.*^{16–18} This model attributes the enhancement of interdiffusion to excess vacancies during the transient process rather than to Si diffusion. While this model is much more relevant to short-time annealing, it still has a major short-coming in that it could not accurately predict the depth-dependence of mixing displayed in the experiments of the authors.

In previous ion mixing studies, the typical period of the superlattice structures employed was 20–40 nm. This type of “long period” superlattice requires a relatively high critical dose to achieve mixing. Consequently, the lateral mixing extent is significant and a higher thermal budget is needed to recover the lattice damage induced during implantation. Obviously, neither high dose nor strong annealing condition is favorable for optimizing the spatial resolution and for preserving the crystal quality. Thus, in this investigation, a “short period” superlattice (7 nm) is employed so that optimization in terms of both low dose and minimal annealing can be achieved. The focused ion beam implantation used in this study features much higher current density than a conventional broad ion beam. It is therefore interesting to determine whether FIB-induced mixing has properties which are

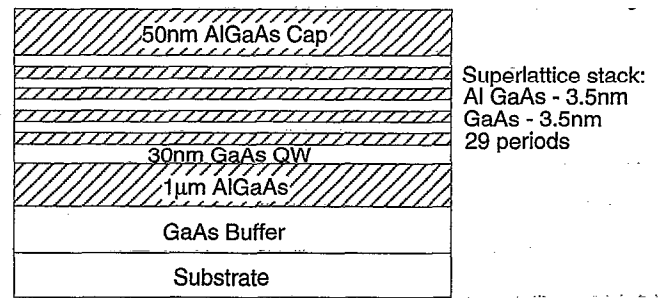


FIG. 1. Schematic of the superlattice structure used in this study. Period of superlattice: 7 nm (3.5 nm+3.5 nm). Al composition in AlGaAs: 0.3. Thickness of superlattice stack: 203 nm (29 periods).

quantitatively different from that with a conventional broad ion beam.

II. EXPERIMENTAL CONDITIONS

The superlattice/quantum structures used in this study were grown by molecular beam epitaxy. The basic structure of the grown samples is shown in Fig. 1. The orientation of the substrates is $\langle 100 \rangle$. The GaAs buffer layer was grown first, followed by an $\text{Al}_x\text{Ga}_{1-x}\text{As}$ cladding layer of 1 μm thickness, a 30 nm GaAs quantum well, a GaAs/ $\text{Al}_x\text{Ga}_{1-x}\text{As}$ superlattice with 7 nm period (2×3.5 nm) and an $\text{Al}_x\text{Ga}_{1-x}\text{As}$ cap layer. The Al composition, x , was approximately 30%.

FIB implantations were performed with a MicroBeam-150 FIB system. The species and energies used for FIB implantation were Si^{++} at 200 and 100 keV. The ~ 100 nm beam diameter and ~ 50 pA ion current yielded a current density of 0.5 A/cm², which is much higher than that of conventional broad ion beams. The beam incident angle was 90° with respect to the sample surface and various doses were chosen. Square regions of 280 $\mu\text{m} \times 280$ μm were implanted in order to be characterized by secondary ion mass spectroscopy (SIMS). Subsequent RTA was performed at 950 °C for 10 s with proximity protection. During RTA, the superlattice samples were sandwiched between two GaAs wafers in a graphite pill box. Forming gas, containing 96% N_2 and 4% H_2 , was introduced during the annealing. This RTA condition was verified to be sufficient for localized mixing in the implanted region, while preserving the original superlattice structure in the unimplanted region.²² The depth profiles of the Al and Si distributions were precisely measured with SIMS.

III. RESULTS

Representative SIMS depth profiles of the Al composition are shown in Figs. 2–4. A comparison of Al concentration depth profiles is shown in Fig. 2 for an as-grown sample, a sample after RTA-only and a sample implanted at 200 keV but not annealed. In principle, the reduction in peak-to-valley ratio of the Al mole fraction in the superlattice beyond that of the as-grown sample reflects the degree of mixing due to either annealing or implantation, or (as shown later) to their combined effect. It is important to point out that the three

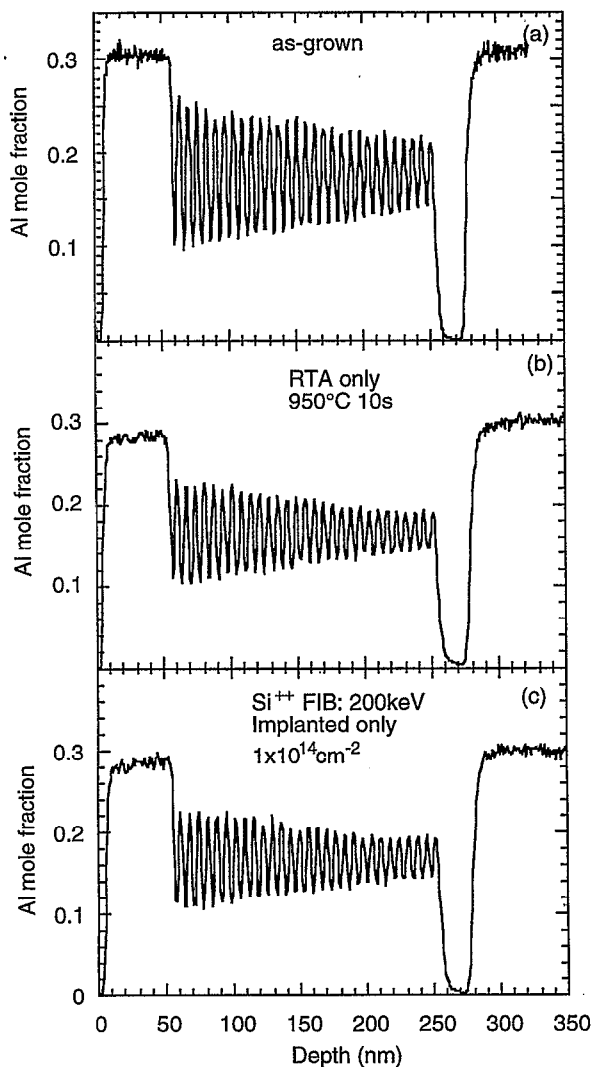


FIG. 2. SIMS depth profiles of Al in superlattices: (a) as-grown, (b) RTA only at 950 °C for 10 s, (c) as-implanted after Si FIB at 200 keV with a dose of $1 \times 10^{14} \text{ cm}^{-2}$.

depth profiles share a less than complete excursion (which should go from zero to 30% mole fraction) of the Al concentration within the superlattice region as well as a tapering of the Al peak-to-valley variation. Both of these effects are thought to be due to limitations of the SIMS technique. The depth resolution of the SIMS profile is around 20 Å. Since the superlattice structure has a period of 70 Å, only a few data points per period are possible. This explains the fact that the maxima and minima of the Al concentration obtained from SIMS are not accurate within the SL layer. In addition, the sputtering process utilized to remove material for depth profiling has the side-effect of gradually exposing fractions of both the GaAs and the AlGaAs sublayers because of film thickness and ion beam nonuniformities over the area analyzed. In turn, this results in the tapered profile observed by us as well as by most workers in the field. The mixing induced by 200 keV Si implantation (Fig. 3), which has a projected range (R_p) deeper than the superlattice stack, is

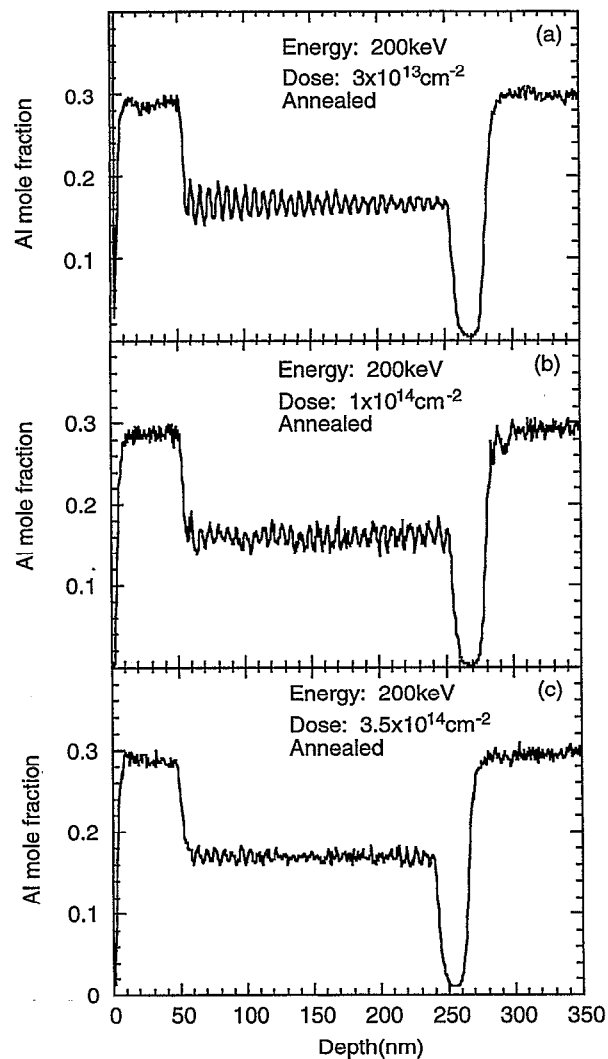


FIG. 3. SIMS depth profiles of Al in superlattices after 200 keV Si FIB implantation and RTA at 950 °C for 10 s with various doses: (a) $3 \times 10^{13} \text{ cm}^{-2}$, (b) $1 \times 10^{14} \text{ cm}^{-2}$, (c) $3.5 \times 10^{14} \text{ cm}^{-2}$.

quite uniform over the entire superlattice region. In contrast, the mixing caused by 100 keV Si ions (Fig. 4), whose R_p is in the middle of the superlattice, is much more depth dependent.

For uniformly mixed samples (those implanted at 200 keV), a statistical calculation was carried out in order to exclude effects introduced during SIMS measurement and to accurately assess the degree of mixing. For these samples, the standard deviation of the Al composition over the entire SL depth was calculated to provide a more accurate measure of the average peak-to-valley ratio. By normalizing the Al standard deviation of an implanted sample to that of its as-grown condition, the degree of mixing can be quantitatively evaluated. A normalized standard deviation (NSD) of 1 represents the as-grown superlattice, while an NSD of zero indicates complete mixing. For convenience, a mixing parameter (MP) was also defined as: $MP = 1 - NSD$.²² Based on this definition, a MP of zero corresponds to as-grown material and a MP of 1 represents complete mixing. For uniformly

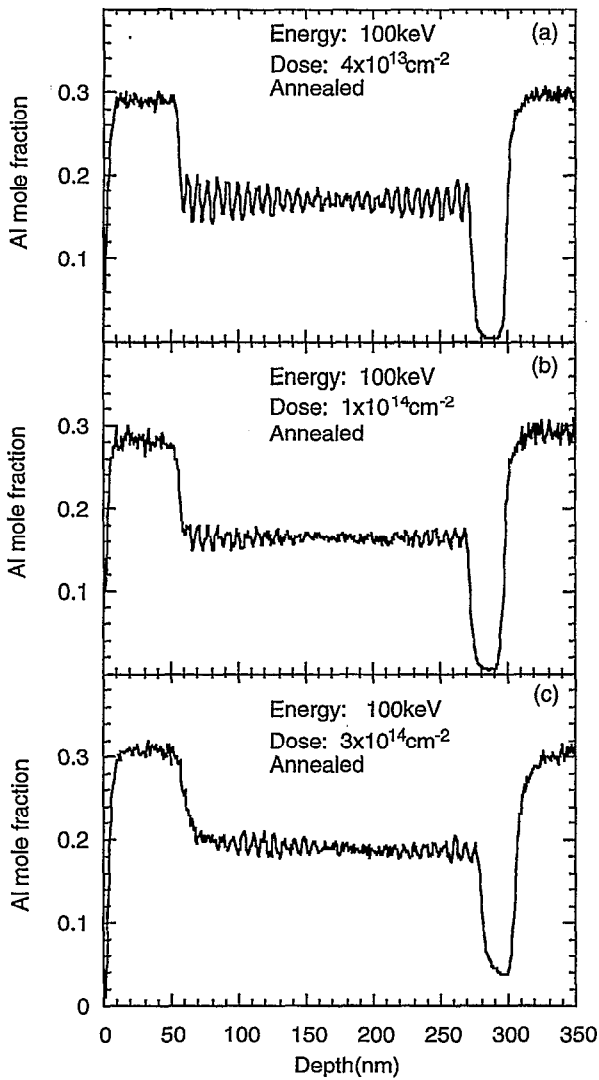


FIG. 4. SIMS depth profiles of Al in superlattices after 100 keV Si FIB implantation and RTA at 950 °C for 10 s with various doses: (a) $4 \times 10^{13} \text{ cm}^{-2}$, (b) $1 \times 10^{14} \text{ cm}^{-2}$, (c) $3 \times 10^{14} \text{ cm}^{-2}$.

mixed samples, the normalized standard deviation, as well as the mixing parameter, were computed over the superlattice region as a function of ion dose, as shown in Fig. 5(a). No significant mixing was induced solely by thermal annealing or ion implantation. However, after implantation and subsequent annealing, the degree of mixing was dramatically enhanced. Even a dose as low as $1 \times 10^{13} \text{ cm}^{-2}$ could generate 72% mixing. A dose of $1 \times 10^{14} \text{ cm}^{-2}$ produced a mixing parameter of 0.89. This is the lowest ion dose necessary for nearly complete mixing reported to date for either FIB or broad beam implantation. This result could be due to the combined effect of FIB implantation, which usually creates more point defects than conventional ion beam implantation, and to the short period superlattice which is more readily mixed. Tripling the dose to $3 \times 10^{14} \text{ cm}^{-2}$ results in an increase in mixing by only 0.05 to a value of 0.94.

In the samples subjected to 100 keV ion implantation, the degree of mixing after RTA is visibly dependent upon the

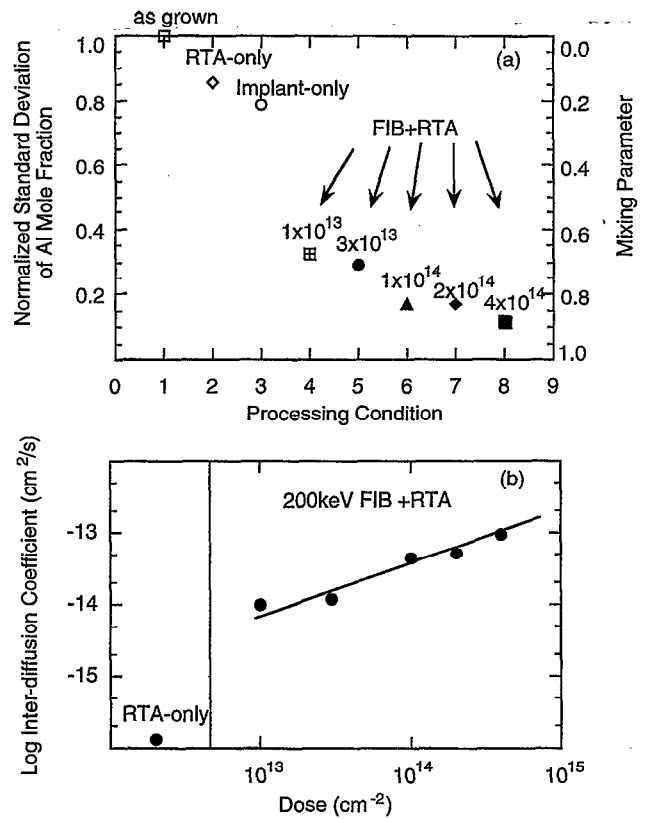


FIG. 5. Mixing effect after 200 keV Si FIB implantation and RTA: (a) normalized standard deviation of Al mole fraction vs various processing conditions, (b) Al-Ga interdiffusion coefficient as a function of dose.

depth, as shown in Fig. 4. A “pinch-off” region, wherein mixing is much more effective than elsewhere, was formed in the superlattice. The length of this pinch-off region was about 80 nm. The degree of mixing in the region is a function of dose. About 80% mixing was observed in the pinch-off region for a dose of $4 \times 10^{13} \text{ cm}^{-2}$, while a dose of $1 \times 10^{14} \text{ cm}^{-2}$ generated almost complete mixing (M.P. >95%).

Figure 6 displays the Si depth profiles measured before and after RTA at 950 °C for 10 s for FIB implantation at energy of 200 keV with a dose of $1 \times 10^{14} \text{ cm}^{-2}$, as well as a TRIM simulation for the same implantation condition. By superimposing the Si depth profiles, one observes that the Si diffusion during the RTA is negligible in the vertical direction. The absence of significant Si diffusion is in good agreement with previous experiments¹⁶ and leads to the following conclusions:

- (1) Si diffusion is not the main vehicle for inter-diffusion during RTA;
- (2) in the RTA time frame, the Si diffusion in the lateral direction should be insignificant.

The diffusion length as well as the inter-diffusion coefficient can be derived based on the Al peak-to-valley ratio obtained from the SIMS profiles as a function of depth.²³ using the error function model,^{15,24,25} the approximate Al-Ga interdiffusion coefficient at 950 °C for 10 s was calculated.

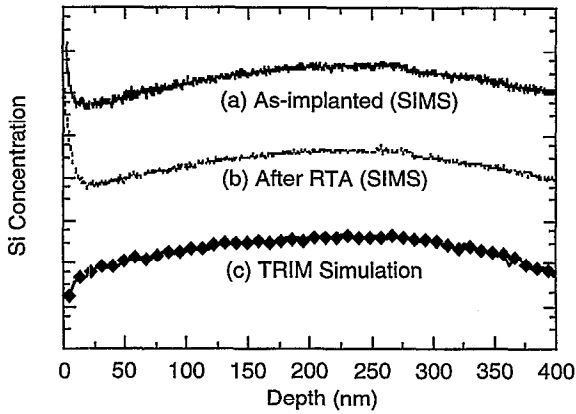


FIG. 6. Comparison of Si depth distributions before and after RTA for Si FIB implantation at 200 keV with dose of $1 \times 10^{14} \text{ cm}^{-2}$. RTA condition: 950 °C, 10 s. The Si profiles were measured with SIMS and simulated with TRIM.

Despite the fact that the period of the superlattice used in this work does not fulfill the condition of thick cladding layer assumed for this model, the calculated interdiffusion coefficient from the RTA-only sample ($1.3 \times 10^{-16} \text{ cm}^2/\text{s}$) is in good agreement with previously published results ($9 \times 10^{-17} \text{ cm}^2/\text{s}$) obtained at the same temperature with furnace annealing in a structure with the same composition but with much thicker barrier layers.¹⁵

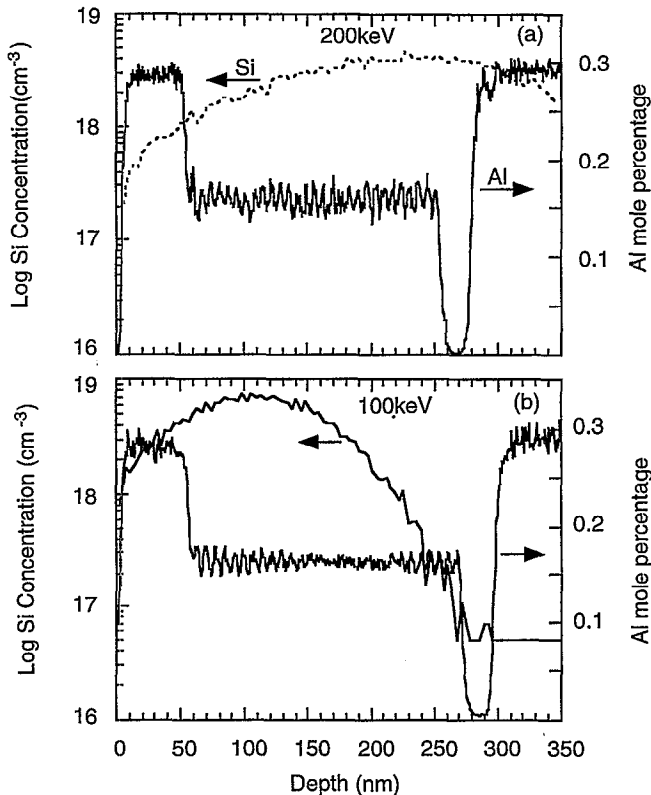


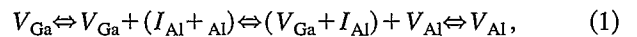
FIG. 7. Si and Al depth profiles of annealed superlattice produced by Si FIB implantation with $1 \times 10^{14} \text{ cm}^{-2}$ dose at energy of: (a) 200 keV, (b) 100 keV.

For uniform mixing (200 keV), the average interdiffusion coefficients are only a function of dose and the results are shown in Fig. 5(b). As an example, the dose of $1 \times 10^{14} \text{ cm}^{-2}$ results in a two-order of magnitude increase in the diffusion coefficient, to a value of $4.5 \times 10^{-14} \text{ cm}^2/\text{s}$, in contrast to $1.3 \times 10^{-16} \text{ cm}^2/\text{s}$ from RTA-only. Similar calculations were made for depth-dependent mixing produced by Si FIB implantation at 100 keV. Si and Al depth profiles for implantation energies of 100 and 200 keV are shown in Fig. 7 for an implantation dose of $1 \times 10^{14} \text{ cm}^{-2}$. Interdiffusion coefficient calculations were performed based on these profiles. As shown in Fig. 8, for 100 keV implantation with a dose of $1 \times 10^{14} \text{ cm}^{-2}$, the interdiffusion coefficient in the pinch-off region, is approximately ten times larger than that obtained in the rest of the superlattice structure. For comparison, the interdiffusion coefficient of uniform mixing produced by implantation at 200 keV with that same dose is also presented in Fig. 8.

IV. ANALYSIS AND MODEL

Based on the experimental results presented above, an understanding of the mechanisms involved in Si implantation-enhanced-mixing has been pursued in order to optimize and precisely control the process of locally selective mixing.

The interdiffusion between AlGaAs and GaAs layers proceeds through point defects.¹ In our case, we assume that the As pressure is high enough to provide an As-rich annealing environment. In this condition, the major point defect associated with Si ion implantation has been suggested²⁰ to be the triply charged vacancy on the Ga site, V_{Ga}^{-3} . Usually, these vacancies are concentrated in the GaAs instead of the AlGaAs layers, since the bond between Al and As is more difficult to break. At annealing temperatures, these defects are mobile and are able to diffuse through the heterointerface in a multi-step process summarized¹ in the following expression:



where V_{Al} and I_{Al} are the Al vacancy and interstitial, respectively.

The attractive interaction between an impurity ion and a charged point defect provides an additional contribution to this process. By using the charged vacancy as a vehicle, the Al-Ga atomic interdiffusion can be significantly enhanced. Three elements play key roles in this process: (1) the As vapor pressure, (2) the doping, (3) the point defect nonequilibrium concentration induced by chemical or physical processes.

Usually, the As vapor pressure affects the interdiffusion process a great deal. The diffusion coefficient for column III atoms (Ga, Al, etc.) can be expressed as:¹

$$D_{\text{III}} = f_1 D_V (P_{\text{As}_4})^{1/4} + f_2 D_I (P_{\text{As}_4})^{-1/4}, \quad (2)$$

where D_V and D_I represent the diffusion coefficient for the column III vacancy and interstitial, respectively. P_{As_4} represents the As vapor pressure. This expression indicates that D_{III} is governed by V_{Ga} for sufficiently high As pressure and

by I_{Ga} for sufficiently low As pressures. The GaAs sandwich structure which we have used in the RTA process provides an As-rich condition and, therefore, the diffusion is column III vacancy dominated diffusion.

Previous studies show that the thermal equilibrium concentration of charged point defects is enhanced by doping, the so-called Fermi-level effect.^{1,3} Those enhanced charged point defects in turn make a significant contribution to the Ga-Al interdiffusion coefficient $D_{\text{Ga-Al}}$, which is approximate equal to D_{Al} and D_{Ga} . According to the Fermi-level effect model, the presence of the dopant (and not necessarily its motion) is the factor enhancing the Ga-Al interdiffusion process. For n -doped material under thermal equilibrium, the equilibrium Al diffusivity³ is given by:

$$D_{\text{Al,eq}} = \left[D_v(n_i) \frac{n}{n_i} \right]^3, \quad (3)$$

where n and n_i are the free electron concentrations of doped and intrinsic material, respectively. In the Fermi-level model, the maximum impurity concentration is associated with the maximum vacancy concentration and hence will induce maximum mixing. This model describes a steady state process and requires a thermal equilibrium circumstance.

In the RTA time frame ($t \sim 10\text{--}30$ s), a large portion of the thermal process has experienced a nonequilibrium state. During this period, the vacancies diffuse in their own sublattice due to the gradient of vacancy concentration created by ion implantation. The Al-Ga interdiffusion is enhanced not only by the presence of excess vacancies but also by the motion of point defects. In order to describe the Al-Ga interdiffusion process during RTA, a model of the transient Al interdiffusion coefficient was proposed by Kahen and Rajeswaran:¹⁸

$$D_{\text{Al}} = D_{\text{Al,eq}} \frac{C_v}{C_{v,\text{eq}}}, \quad (4)$$

where C_v and $C_{v,\text{eq}}$ represent the total transient and thermal equilibrium vacancy concentration at the annealing temperature. The transient defect model described in Eq. (4) suggests that the excess vacancy concentration controls the interdiffusion coefficient, which in turn determines the degree of intermixing.

However, the transient diffusion model of Kahen and Rajeswaran does not correctly predict¹⁸ some aspects of interdiffusion, especially at depths greater than R_p . From the SIMS profiles for 100 keV Si implanted superlattice (see Fig. 4), the mixing at depths from ~ 150 nm to 220 nm is much more effective than elsewhere in the superlattice structure. With increasing dose, the peak-to-valley ratio in this region is significantly decreased and eventually a complete pinch-off is formed at depth of 170 nm. It is important to note that the depth of this maximum mixing did not coincide with the maximum of either the Si (at ~ 100 nm) or vacancy concentrations. The vacancy, as well as the impurity, concentration is clearly still an important factor here because the average degree of mixing over the entire superlattice is proportional to the dose. However, it is evident that in the pinch-off region the mixing is no longer exclusively dominated by either the impurity concentration or the vacancy concentration.

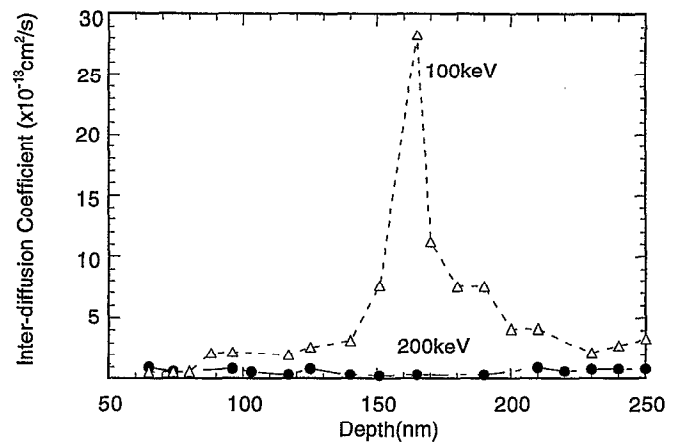


FIG. 8. Al-Ga interdiffusion coefficient as function of depth for FIB implantation with dose of $1 \times 10^{14} \text{ cm}^{-2}$ at 100 and 200 keV after 950 °C, 10 s RTA.

Similar depth-dependent phenomena have been observed by a number of groups^{13,16-18} from various superlattice structures and processing conditions, including the authors of the transient model. In the results reported by Kahen *et al.*,²⁵⁻²⁷ the mixing abruptly increases in the region that is beyond the R_p and cannot be interpreted by the transient defect model they proposed for the RTA situation.

The depth distribution of Si atoms and vacancies produced by the implantation experiments were simulated with the TRIM²⁷ program. An example for a dose of $1 \times 10^{14} \text{ cm}^{-2}$ is shown in Fig. 9(a). Si depth profiles computed by TRIM were in good agreement with those measured by SIMS. To explore the mechanism of the enhanced mixing in the pinch-off region, we have calculated the second derivative of the vacancy concentration (SDVC)

$$\text{SDVC} = \frac{\partial^2 C_v(x,t)}{\partial x^2}. \quad (5)$$

The calculated SDVC depth distribution and the corresponding interdiffusion coefficient are shown in Figs. 9(b) and 9(c) for the dose of $1 \times 10^{14} \text{ cm}^{-2}$. From Fig. 9(b), one can clearly note that the pinch-off mixing takes place in the region where SDVC is positive. Furthermore, the pinch-off point coincides with the peak SDVC level. In another aspect, Fig. 9(c) shows that interdiffusion is greatly enhanced by a positive SDVC.

Following the approach of Kahen *et al.*,¹⁶⁻¹⁸ the vacancy concentration time- and space-dependence are interrelated by

$$\frac{\partial C_v(x,t)}{\partial t} = D_v \frac{\partial^2 C_v(x,t)}{\partial x^2} - \frac{[C_v(x,t) - C_{v,\text{eq}}]}{\tau}, \quad (6)$$

where τ is the decay time constant of vacancies. The first term on the right side of the equation represents the vacancy gradient (the cause of diffusion) and the second term represents the vacancy recombination. The recombination term will always cause a reduction of the vacancy concentration. Near the top surface, where SDVC is large and negative and $(C_v - C_{v,\text{eq}})$ is also very large, the sign of $\partial C_v/\partial t$ is negative and its amplitude is large. This would indicate a rapid de-

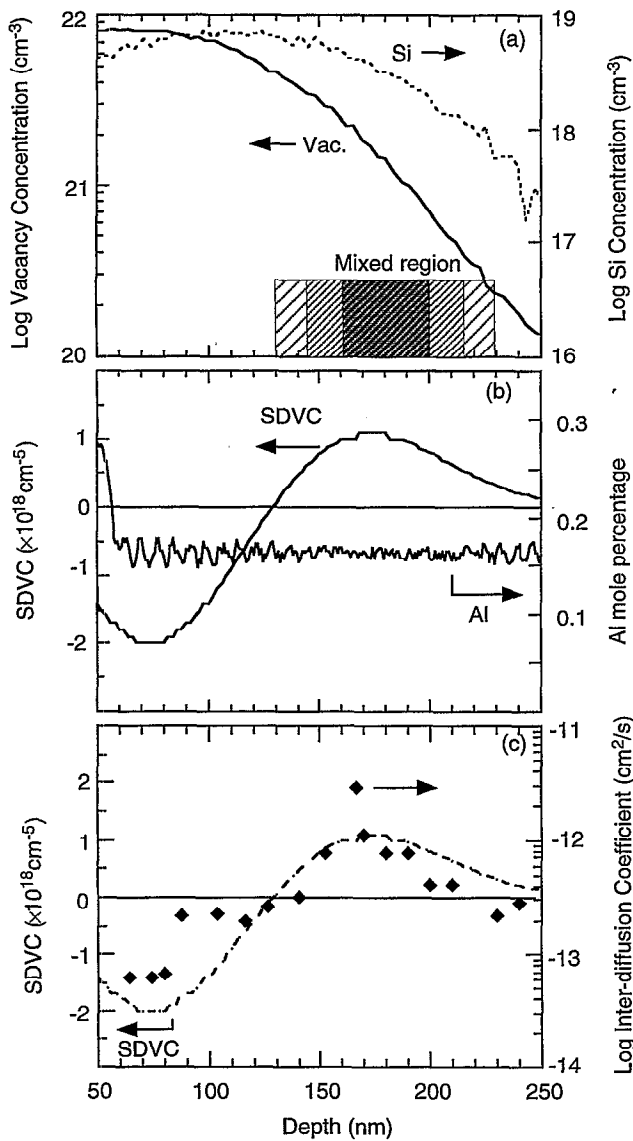


FIG. 9. Mechanism analysis of depth-dependent mixing in superlattice after Si FIB (100 keV, $1 \times 10^{14} \text{ cm}^{-2}$) implantation and RTA: (a) vacancy and Si ions depth profiles, (b) SDVC and Al profiles, (c) SDVC and interdiffusion coefficient.

crease in the vacancy concentration in this region. At values of depth for which SDVC is positive, the sign of $\partial C_v(x,t)/\partial t$ is determined by the subtraction in the right side of Eq. (6). When $D_v[\partial^2 D_v(x,t)/\partial x^2] - [C_v(x,t) - C_{v,eq}]/\tau > 0$, a positive $\partial C_v(x,t)/\partial t$ is obtained, indicating that the vacancies are injected into the region. This is presumably the pinch-off region, where SDVC is large and positive and a high level of mixing occurs, as shown in Fig. 9(b). As one proceeds deeper into the SL stack, SDVC continues to be positive but its amplitude decreases, as does that of the vacancy concentration. Since an absence of mixing is observed in the pinch-off region, it is assumed that here $\partial C/\partial t$ is determined by the decreasing SDVC.

The vacancy decay time constant is of the order of a few seconds.¹⁷ Therefore, in the context of rapid thermal annealing, increasing the anneal time beyond 10 s will not signifi-

cantly increase the level of mixing. However, this conclusion does not apply to furnace annealing because of significant impurity diffusion^{1,3,21} which occurs during a much longer time frame.

Turning our attention again to the comparison between SDVC and the interdiffusion coefficient as a function of depth [Fig. 9(c)], we assume that the more sharply peaked profile of the interdiffusion coefficient is due to the reducing effect of vacancy recombination on vacancy injection.

Based on these assumptions, our analysis suggests that the Al-Ga interdiffusion is enhanced by the vacancy injection that takes place in the region where SDVC is positive and sufficiently large. This injection, generated by the presence of a gradient in the transient vacancy concentration (and modified by the recombination of excess vacancies) is presumably responsible for the enhanced mixing occurring in the pinch-off region.

Through curve fitting, an exponential form of the interdiffusion coefficient is derived as a function of SDVC:

$$D_{\text{Al}} = \beta \cdot \exp\left(\alpha \frac{\partial^2 C_v(x,t)}{\partial x^2}\right), \quad (7)$$

where α is a constant. β includes the nonequilibrium effect of transient-enhanced interdiffusion¹⁸ during RTA which was previously considered. The exponential term represents the enhanced interdiffusion effect of vacancy injection. $D_{\text{Al,eq}}$ is the interdiffusion coefficient under equilibrium condition and is proportional to the impurity concentration.

Considering the experimental model described by Eq. (7) and the conventional transient defect model given in Eq. (4), we propose the following expression for the Al-Ga interdiffusion coefficient in the time frame of RTA:

$$D_{\text{Al}} = D_{\text{Al,eq}} \frac{C_v}{C_{v,eq}} \cdot \exp\left(\alpha \frac{\partial^2 C_v(x,t)}{\partial x^2} \varphi\right), \quad (8)$$

where the term φ represents the influence of vacancy recombination.

Equation (8) indicates that the Al-Ga interdiffusion is significantly affected by the motion of vacancies that occurs during the early period of rapid thermal annealing due to the implantation-induced gradient. In this period, nonequilibrium processes take place. Point defects, presumably charged vacancies, diffuse quickly in their own sublattice, while Si diffusion is not yet significant. The interdiffusion is enhanced at all the depths by excess charged vacancies (V_{Ga}^{-3}) due to doping, and it is most strongly enhanced in the region into which the vacancies are injected. The vacancy injection greatly enhances the Al-Ga interdiffusion and becomes a decisive factor in the nonequilibrium period of annealing. However, this vacancy injection process will be saturated in a few seconds because a thermal equilibrium of the vacancy concentration profile will be established. Therefore, the mixing usually does not increase appreciably as the annealing time is increased beyond a certain point.¹⁶ When the annealing time is long enough (as in furnace annealing), the mixing process is under dynamic equilibrium and it is dominated by the impurity concentration as well as impurity diffusion, as described in the Fermi-level effect and impurity diffusion models.

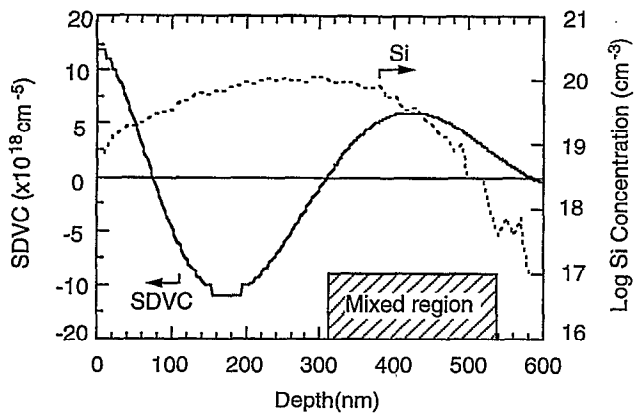


FIG. 10. TRIM-simulated depth profiles of Si concentration and SDVC for 220 keV Si^+ implantation with dose of $3 \times 10^{15} \text{ cm}^{-2}$ in GaAs/AlGaAs superlattice (period: 20 nm+20 nm). The thickness of superlattice stack is $1.6 \mu\text{m}$ and complete mixing occur in the marked region. The experiment and SIMS profiles were published by Lee *et al.* (see Ref. 27).

In the regions where SDVC is negative, the exponential term in Eq. (8) is less than unity. In spite of possibly high vacancy concentrations in these regions, the interdiffusion coefficient is limited as a result of the multiplication product by a small exponential term. For example, in the case of 200 keV implantation (see Fig. 3), the overlap of the vacancy concentration peak and negative SDVC values results in a relatively uniform mixing.

Equation (8), however, only provides a mathematical description of the mixing process observed experimentally. Intuitively, one would have expected that high values of positive *and* negative SDVC would result in enhanced mixing, as both conditions imply a high rate of vacancy diffusion. A possible explanation for this discrepancy may be related to the fact that the negative SDVC depth range coincides with the highest level of vacancy concentration ($\sim 8 \times 10^{21} \text{ cm}^{-3}$), which is located in the near-surface region. Indeed, at this level of defects, this region is most likely nearly amorphous. It is known¹³ that at high concentrations, vacancies coalesce and form dislocations and other extended defects. In turn, these defects may prevent intermixing. We have searched for an alternative explanation for this phenomenon, which would be solely tied to the polarity of the SDVC. However, we have not been able to identify a suitable candidate.

As a verification of our model, we have calculated the impurity and vacancy distributions of a different superlattice structure and implantation condition, in which a strong depth-dependent mixing was also observed, reported by Lee *et al.*,¹⁶ and Kahen *et al.*^{17,18} The results are shown in Fig. 10. Since the period of the superlattice used here was relatively thick (40 nm), the required dose for mixing was considerably higher than in our case. The energy of implanted Si^+ was 220 keV, which corresponds to an R_p of 280 nm. Rapid thermal annealing was subsequently performed. Similar to the results we reported above, the mixing only occurred from a depth of ~ 320 to 520 nm, in other words beyond the peak of both Si and vacancy concentrations. The position of the mixed region is observed to clearly coincide

with the range of positive SDVC values. This result strongly supports the vacancy injection mechanism we are proposing.

V. DISCUSSION

In general, the interdiffusion is dominated by either a single or by combined mechanisms in different circumstances. A brief discussion is given in this section regarding interdiffusion in several most common situations.

A. Interdiffusion in intrinsic superlattice

In this case, the carrier concentration is equal to the intrinsic concentration leading to a constant vacancy concentration and, thus, to an SDVC of zero [from Eq. (5)]

$$n = n_i \rightarrow C_v = C_{v,\text{eq}} \rightarrow \text{SDVC} = 0. \quad (9a)$$

The Al interdiffusion is also constant with depth, and is given by thermal equilibrium value

$$D_{\text{Al}} = D_{\text{Al,eq}} = D_{\text{Al}}(n_i) = D_v(n_i). \quad (9b)$$

For example, for either furnace annealing¹⁵ or RTA¹⁹ at 950 °C of intrinsic superlattice structure, similar results were obtained as $D_{\text{Al}} = D_{\text{Al}}(n_i) \approx 1 \times 10^{-16} \text{ cm}^2/\text{s}$.

B. Interdiffusion in uniformly doped superlattice

A uniform dopant distribution usually results from doping during crystal growth. In this situation, $\text{SDVC} = 0$. For FA, the process is under thermal equilibrium and can be accurately described by the Fermi-level model. Furthermore, this approach can even be satisfactorily applied to RTA results,³ since the major nonequilibrium processes such as vacancy injection are not involved. According to Eq. (8),

$$D_{\text{Al}} = \frac{C_v}{C_{v,\text{eq}}} D_{\text{Al,eq}} = D_{\text{Al}}(n). \quad (10)$$

In this case, $C_v/C_{v,\text{eq}}$ is constant throughout the entire depth and approaches unity as thermal equilibrium is reached.

C. Interdiffusion during FA with gradient doping

This is the most well-studied case. Because of FA, a comparatively long time thermal process is experienced. At the onset of annealing, point defects diffuse and vacancy injection will enhance the interdiffusion. However, because the temperature employed in furnace annealing is relatively low, this vacancy injection has less impact on the ultimate outcome. After a short period of time, the dynamic equilibrium will be established, $\text{Si}^+ - \text{V}^-$ pairs will be formed and will diffuse toward the inside. The Fermi-level model is also applicable because Si diffusion is relatively slow at typical FA temperatures. As a result, the interdiffusion will still mainly depend on the impurity concentration. A threshold Si concentration for mixing was found to be at $3 \times 10^{18} \text{ cm}^{-3}$.^{7,9}

D. Interdiffusion during RTA with gradient doping

In most instances of rapid thermal annealing period, steady state is not attained due to significant SDVC and high anneal temperature. This case is a nonequilibrium process and the mixing is dominated by the combination of vacancy

injection, transient vacancy concentration, and impurity concentration. At all depths within the superlattice, the interdiffusion is enhanced with respect to the undoped superlattice case. The greatest enhancement takes place in the vacancy injection region. Equation (8) provides the description of this most complex interdiffusion process. The effectiveness of this equation is verified by the depth-dependent mixing presented in Sec. III of this article and the results published by other groups.^{13,16-18}

VI. OPTIMIZATION OF MIXING PROCESS

The optimization of selective mixing with minimal lateral profile can be achieved under the following considerations:

- (1) employing a short period superlattice;
- (2) using rapid thermal annealing with minimal thermal budget;
- (3) using low dose impurity implantation;
- (4) minimizing the dose by properly utilizing the enhancement in vacancy injection region.

In our experiments, the short period superlattice with a 7 nm period is proven to be quite effective in terms of mixing with low dose. Meanwhile, the RTA condition of 10 s at 950 °C is capable of rendering the implanted superlattice region mixed and removing the damage induced by implantation with moderate dose.²² The dose of 1×10^{14} cm⁻² at an energy of 200 keV provides a satisfactory mixing result throughout the entire depth of the superlattice. The same dose at an energy of 100 keV leads to a complete mixing in the pinch-off region. The selection of ion energy and dose is based on several considerations:

- (a) trade-off between more complete mixing with higher dose and smaller lateral profile with lower dose;
- (b) smaller lateral ion straggling at lower energy and finer focused ion beam at higher energy;
- (c) more complete mixing but relatively small mixing depth with lower energy and less complete but more uniform mixing with higher energy.

The optimization can therefore be carried out with respect to the requirement of a specific application. As an example, we have demonstrated the fabrication of a DBR laser grating structure by periodically mixing the superlattice using a focused Si ion beam at 200 keV with dose of a 1×10^{14} cm⁻² and subsequent RTA. The details of this result were presented elsewhere.¹⁹

VII. SUMMARY

In summary, we have studied the Si⁺⁺ FIB-induced mixing of an Al_{0.3}Ga_{0.7}As/GaAs superlattice structure. A fairly complete mixing can be achieved with a relatively low dose at a certain depth. This result can be utilized to minimize lateral spread, reduce damage, and achieve depth control.

The mechanism for the depth-dependence and pinch-off mixing effect were discussed. Nonequilibrium vacancy injection has been suggested as being responsible for the high degree of mixing in the pinch-off region. Based on experimental results, a theoretical model has been proposed to describe the inter-diffusion as well as the mixing process in the time scale of RTA.

ACKNOWLEDGMENTS

The authors would like to thank R. Kolbas for the MBE growth, S. Novak for the SIMS measurement and many related discussions, and A. G. Choo, J. T. Boyd, and H. E. Jackson for many useful discussions. Partial support for this work from the National Science Foundation and the Materials Directorate, Wright Laboratory at the Wright-Patterson Air Force Base is acknowledged.

- ¹D. G. Deppe and N. Holonyak, Jr., *J. Appl. Phys.* **64**, R93 (1988).
- ²K. Ishida, E. Miyauchi, T. Morita, T. Takamori, T. Fukunaga, H. Hashimoto, and H. Nakashima, *Jpn. J. Appl. Phys.* **26**, L285 (1987).
- ³T. Y. Tan, U. Gosele, and S. Yu, *Crit. Rev. Solid State Mater. Sci.* **17**, 47 (1991).
- ⁴E. Dobisz, R. Marrian, H. Craighead, S. Schwarz, and J. Harbison, *J. Vac. Sci. Technol. B* **7**, 2053 (1989).
- ⁵K. Ishida, K. Matsui, T. Fukunaga, J. Kobayashi, T. Morita, E. Misauchi, and H. Nakashima, *Appl. Phys. Lett.* **51**, 109 (1987).
- ⁶J. Kobayashi, T. Fukunaga, K. Ishida, H. Nakashima, J. Flood, G. Bahir, and L. Merz, *Appl. Phys. Lett.* **50**, 519 (1987).
- ⁷J. Kobayashi, M. Nakajima, Y. Bamba, T. Fukunaga, K. Matsui, K. Ishida, H. Nakashima, and K. Ishida, *Jpn. J. Appl. Phys.* **25**, L385 (1986).
- ⁸J. Kobayashi, M. Nakajima, T. Fukunaga, T. Takamori, K. Ishida, H. Nakashima, and K. Ishida, *Jpn. J. Appl. Phys.* **25**, L736 (1986).
- ⁹K. Matsui, J. Kobayashi, T. Fukunaga, K. Ishida, and H. Nakashima, *Jpn. J. Appl. Phys.* **25**, L651 (1986).
- ¹⁰M. Kawabe, N. Matsuura, N. Shimizu, F. Hasegawa, and Y. Nannichi, *Jpn. J. Appl. Phys.* **23**, L623 (1984).
- ¹¹Y. Hirayama, Y. Horikoshi, and H. Okamoto, *Jpn. J. Appl. Phys.* **23**, 1568 (1984).
- ¹²T. Venkatesan, S. Schwarz, D. Hwang, R. Bhat, M. Koza, H. Yoon, P. Mei, Y. Arakawa, and A. Yariv, *Appl. Phys. Lett.* **49**, 701 (1986).
- ¹³S. A. Schwarz, T. Venkatesan, R. Bhat, M. Koza, H. Yoon, Y. Arakawa, and P. Mei, *Mater. Res. Soc. Symp. Proc.* **56**, 321 (1986).
- ¹⁴S. Schwarz, T. Venkatesan, D. Hwang, H. Yoon, R. Bhat, and Y. Arakawa, *Appl. Phys. Lett.* **50**, 281 (1987).
- ¹⁵T. E. Schlesinger and T. Kuech, *Appl. Phys. Lett.* **49**, 519 (1986).
- ¹⁶S. T. Lee, G. Braunstein, P. Fellingner, K. Kahen, and G. Rajeswaran, *Appl. Phys. Lett.* **53**, 2531 (1988).
- ¹⁷K. Kahen, G. Rajeswaran, and S. Lee, *Appl. Phys. Lett.* **53**, 1635 (1988).
- ¹⁸K. Kahen and G. Rajeswaran, *J. Appl. Phys.* **66**, 545 (1989).
- ¹⁹A. J. Steckl, P. Chen, A. Choo, H. Jackson, J. Boyd, A. Ezis, P. Pronko, S. Novak, and R. Kolbas, *Mater. Res. Soc. Symp. Proc.* **281**, 319 (1993).
- ²⁰M. Greiner and F. Gibbons, *Appl. Phys. Lett.* **44**, 751 (1984).
- ²¹M. Greiner and J. Gibbons, *J. Appl. Phys.* **57**, 5181 (1985).
- ²²A. Steckl, P. Chen, A. Choo, H. Jackson, J. Boyd, P. Pronko, A. Ezis, and R. Kolbas, *Mater. Res. Soc. Symp. Proc.* **240**, 703 (1992).
- ²³P. Mei, Y. Yoon, T. Venkatesan, S. Schwarz, and J. Harbison, *Appl. Phys. Lett.* **50**, 1823 (1987).
- ²⁴K. Kash, B. Tell, P. Grabbe, E. Dobisz, H. Craighead, and M. Tamargo, *J. Appl. Phys.* **63**, 190 (1987).
- ²⁵L. Chang and A. Koma, *Appl. Phys. Lett.* **29**, 138 (1976).
- ²⁶L. Pavesi, N. Ky, J. Ganiere, F. Reinhart, N. Baba-Ali, I. Harrison, B. Tuck, and M. Henini, *J. Appl. Phys.* **71**, 2225 (1992).
- ²⁷J. F. Ziegler, J. P. Biersack, and U. Littmark, *Stopping and Range of Ions in Matter* (Pergamon, New York, 1988), Vol. 1.